Plasma Chem Plasma Process (2014) 34:239–257
DOI 10.1007/s11090-013-9513-1

ORIGINAL PAPER

On the LPCVD-Formed SiO_2 Etching Mechanism in $CF_4/Ar/O_2$ Inductively Coupled Plasmas: Effects of Gas Mixing Ratios and Gas Pressure

Jinyoung Son · Alexander Efremov · Inwoo Chun · Geun Young Yeom · Kwang-Ho Kwon

Received: 5 June 2013 / Accepted: 2 December 2013 / Published online: 23 January 2014

Abstract An investigation of etching mechanism of low-temperature SiO_2 thin films in $CF_4/Ar/O_2$ inductively coupled plasmas at constant input power (900 W) and bias power (200 W) was carried out. It was found that that the variations of Ar/O_2 mixing ratio (0–50 %) at constant 50 % CF_4 fraction as well as the change in gas pressure (4–10 mTorr) resulted in non-monotonic SiO_2 etching rates. The zero-dimensional plasma model with Langmuir probe diagnostics data provided the detailed information on formation-decay kinetics for plasma active species. The model-based analysis of etching kinetics showed that these effects were not connected with the non-monotonic change of fluorine atom density (as was found in several works for the binary CF_4/O_2 system), but resulted from the decrease in reaction probability and with the transition from neutral-flux to ion-flux-limited regimes of ion assisted chemical reaction.

Keywords Low-temperature SiO_2 · CF_4 plasma · Diagnostics · Modeling · Etching mechanism

Introduction

Silicon dioxide (SiO_2) played an important role in advanced electronic device technology in all temporal steps of its development. Being originally used as the gate dielectric, now

J. Son (✉) · I. Chun · K.-H. Kwon
Department of Control and Instrumentation Engineering, Korea University, Sejong 339-700, South Korea
e-mail: son_jy@korea.ac.kr

A. Efremov
Department of Electronic Devices and Materials Technology, State University of Chemistry and Technology, 7 F. Engels St., 153000 Ivanovo, Russia

G. Y. Yeom
Department of Advanced Materials Science and Engineering, Sungkyunkwan University, Suwon 440-746, South Korea

the SiO_2 lost the leading role in this field because of numerous high-k materials providing both lower dimensions and better characteristics for field-effect transistors [1, 2]. Currently, the interest to SiO_2 has been renewed by the development of micro-electro-mechanical systems (MEMS). In MEMS technology, the basic method for producing the SiO_2 layers is the low pressure chemical vapor deposition (LPCVD). The advantage of the LPCVD process compared with the thermal oxidation, except the much lower process temperatures, is the possibility of the SiO_2 growth rate adjustments by the temperature, pressure and composition of gas mixture [3]. Also, the LPCVD-formed SiO_2 (so-called the low temperature oxide, LTO) requires no polishing because it faithfully reproduces the structure of the underlying layers [4]. Since the MEMS technology includes a combination of deposition and etching steps, the development of the dry etching process for LTO films for the required surface micromachinning is an important task to be solved in a nearest future. Similarly to the conventional electronic device technology, the fluorine-containing, particularly the CF_4-based plasmas, are normally used for this purpose [4].

From numerously published works (for example, from Refs. [5–15]), the basic features of the SiO_2 etch process in the CF_4-containing plasmas can be summarized as follows:

1. The dominant role in chemical etching pathway belongs to F atoms. The effect from CF_x radical is much smaller and appears only through their ion-assisted dissociation of the surface [5–7]. The role of F_2 molecules which are formed in the CF_4-based plasmas with the densities compared with those for F atoms [13] can also be ignored due to the three order of magnitude lower reaction probability [14, 15].
2. The etching process needs ion bombardment with the energies more than 150–200 eV in order to sputter the low volatile fluorinated layer. In this case, the etching process occurs in the reaction-rate-limited etching regime, and the etching rate follows the behavior of F atom density [6, 7, 10–12].
3. The rate of spontaneous (thermally-activated) reaction of F atoms with SiO_2 surface at near-to-room temperatures can be neglected. The dissociative adsorption of CF_x radicals on SiO_2 does not occur [11–13].
4. In the CF_4/O_2 plasmas, the SiO_2 etching rate shows a maximum at 30–40 % O_2. Such effect appears in plate-parallel reactive ion etching (RIE) reactors at relatively high pressures (100–500 mTorr) as well as in the inductively coupled plasma (ICP) systems operating at pressures less than 10 mTorr [5–8]. Normally, the non-monotonic etching rate is attributed to the same behavior of F atom density and to the effective gasification of the fluorocarbon polymer layer in the presence of the active oxygen. The reasonability of the first assumption was repeatedly confirmed by several works on both diagnostics and modeling of CF_4/O_2 plasmas [16–20].

However, when analyzing the existing works, one can conclude that the effect of oxygen on SiO_2 etching rate, plasma parameters, and composition is well studied only for the binary CF_4/O_2 gas mixture at constant total gas pressure. Accordingly, an increase in the O_2 mixing ratio is accompanied by a proportionally decreasing CF_4 fraction. At the same time, modern plasma etching technology involves three- or more component gas mixture, for example CF_4/O_2/Ar. Kimura and Hanaki [21] have reported the experimental study of CF_4/O_2/Ar ICP with variable CF_4 fractions in a feed gas. They found that the behaviors of plasma parameters and F atoms density versus gas mixing ratio are quite similar to those obtained for the CF_4/O_2 plasma. From this work, it can be understood also that the metastable Ar atoms do not influence the dissociation kinetics for mixture components. At the same time, the three-component systems provide much more pathways for the changes in gas mixing ratios in order to obtain the optimal process conditions. For

example, one can fix the fraction of CF_4, but change only the ratio between O_2 and Ar. It is clear that, since the composition of the feed gas is different compared with simple CF_4/O_2 mixture, some principal differences in plasma parameters [through the electron energy distribution function (EEDF) and mean electron energy], densities of plasma active species (through the electron impact and atom-molecular kinetics) and thus, in the SiO_2 etching mechanism which can take place. That is why, the relationships between plasma parameters, plasma composition, and SiO_2 etching mechanism for the three component CF_4/O_2/Ar gas mixture need additional investigations.

The main goal of this work was to investigate how the change in O_2/Ar mixing ratio at constant CF_4 fraction in the CF_4/O_2/Ar gas mixture and the change of gas pressure influence the etching characteristics of low temperature SiO_2 films through the changes of plasma parameters and plasma composition. Also, we attempted the model-based analysis of the SiO_2 etching mechanisms for understanding the behavior of etching rate versus chosen operating parameters that serves for creating the basis for the further process optimization.

Experimental Part

Experimental Setup and Procedures

The SiO_2 films were deposited on Si(100) substrates using the LPCVD technique in E1550HT Diffusion furnace. The precursor gases were SiH_4 and O_2 with the flow rates of 160 and 260 sccm, respectively. The process temperature was 425 °C, and the total gas pressure was 160 mTorr. The final thickness of the LTO films was about 500 nm.

Both etching and plasma diagnostics experiments were performed in planar ICP reactor. The reactor had a cylindrical ($r = 15$ cm) chamber made from the anodized aluminum. The 5-turns copper coil with a diameter of 29 cm was connected to the 13.56 MHz power supply and located above the 10 mm thick-horizontal quartz window on the top side of the chamber. A distance (l) between the window and the bottom electrode used as a substrate holder was 12.8 cm. The bottom electrode was connected to 12.56 MHz power supply to maintain a negative dc bias voltage (U_{dc}). The temperature of the bottom electrode was stabilized at 17 °C using the water-flow cooling system.

For the effect of gas mixing ratio, the experiments were performed at fixed total gas flow rate ($q = 40$ sccm), gas pressure ($p = 6$ mTorr), bias power ($W_{dc} = 200$ W) and input power ($W_{inp} = 900$ W). The last value corresponds to the input power density $w_{inp} = W_{inp}/\pi r^2 l$of 0.9 W/cm^3. The initial compositions of the $CF_4/Ar/O_2$ mixtures were set by adjusting the flow rates of the corresponding gases. In these experiments, the CF_4 flow rate q_{CF_4} was fixed at 20 sccm while O_2 and Ar were mixed with various ratios within $q_{O_2} + q_{Ar} = 20$ sccm. Accordingly, the fraction of CF_4 in the initial gas mixture $y_{CF_4} = q_{CF_4}/q$ was always 0.5, and the remaining half was represented by the different amounts of O_2 and Ar. For the effect of gas pressure, the parameters q, W_{inp} and W_{dc} were fixed at 40 sccm, 900 W and 200 W, respectively. The pressure was changed in the range of 4–10 mTorr. In this case, two basic gas mixtures were investigated. These were the Ar-rich plasma (50 % CF_4 + 38 % Ar + 12 % O_2) and O_2-rich plasma (50 % CF_4 + 12 % Ar + 38 % O_2).

For etching experiments, the samples with the size of about 2 × 2 cm^2 were placed in the center of the bottom electrode. The SiO_2 etched depths were measured using a surface

profiler (Alpha-step 500, Tencor). For this purpose, we developed the line striping of the PR (AZ1512, positive) with the line width/spacing ratio of 2 μm/2 μm. The initial thickness of the PR layer was about 1.5 μm.

Plasma diagnostics was carried out by double Langmuir probe (LP) (DLP2000, Plasmart Inc.). The probes were installed through a hole on the sidewall of the reactor chamber at 5.7 cm above the bottom electrode and centered in a radial direction. The output data were the electron temperature (T_e), ion current density (J_+), floating potential (U_f) and total positive ion density (n_+). The treatment of *I–V* curves was based on the Johnson and Malter's double probes theory [22] and the Allen-Boyd-Reynolds (ABR) approximation [23] for the ion saturation current density without accounting for negative ions. All these assume $J_+ \approx 0.61 e n_+ \upsilon$, where υ is the ion Bohm velocity. Earlier, it was shown that such an approach works not bad even for more electronegative plasmas, for example, for the Cl_2-based ones [24, 25].

Plasma Modeling

In order to obtain the data on densities and fluxes of plasma active species, we used a simplified zero-dimensional model with Maxwellian EEDF and with the experimental data on T_e and n_+ as input parameters [20, 24, 25]. Though the real EEDFs are not exactly Maxwellian, such simplification for the CF_4-based low-pressure ($p < 50$ mTorr) ICPs provides the reasonable agreement between the results of plasma diagnostics and modeling [21, 25–28]. Also for simplicity, we did not account for the negative ion chemistry assuming $n\_/n_e \ll 1$ and $n_e \approx n_+$. The reasonability of such assumption for the given set of experimental conditions follows from the data of Refs. [16, 21, 25]. Particularly, in our previous study [25], it was found that $n\_/n_e \sim 0.3$ for pure CF_4 plasma and $\sim$0.1 for 50 % CF_4 + 50 % Ar gas mixture at $p = 15$ mTorr and $w_{inp} = 0.8$ W/cm^3. Kimura and Hanaki [21] have measured $n\_/n_e \sim 0.2$ in 30 % CF_4 + 70 % Ar plasma for $p = 30$ mTorr and $w_{inp} = 0.7$ W/cm^3. Another Kimura's work [16] reported about $n\_/n_e \sim 0.1$ for pure CF_4, $\sim$0.13 for 50 % CF_4 +50 % O_2 and $\sim$0.22 for pure O_2 plasma at $p = 8$ mTorr and $w_{inp} = 0.8$ W/cm^3. Since all these values relate to higher pressures and lower power densities than those used in the present study, one can surely assume that, in our case, $n\_/n_e < 0.1$.

The steady-state ($dn/dt = 0$) densities of neutral species were obtained from the system of chemical kinetics equations in a general form of $R_F - R_D = (k_s + 1/\tau_R)n$, where R_F and R_D are the volume-averaged formation and decay rates in bulk plasma for a given type of species, n is their density, k_S is the first-order heterogeneous decay rate coefficient, and $\tau_R = \pi r^2 lp/q$ is the residence time. The list of the processes included in the model is given in Table 1. The rate coefficients for electron impact reactions (R1–R20) were calculated using the fitting expressions as functions of T_e [16, 27, 28] in a form of $k = AT_e^B \exp(-C/T_e)$k = $\mathrm{AT_e^B exp(-C/T_e)}$. The rate coefficients for R21–R60 were taken from the NIST database [29] for the gas temperature (T) of 700 K. The last was assumed to be independent on the variable operating parameters. The rate coefficients for heterogeneous loss of atoms and radicals R61–R67 were taken similarly to Ref. [24] as

$$k_S = \left[\left(\Lambda^2/D\right) + (2r/\gamma\upsilon_T)\right]^{-1}, \quad (1)$$

where D is the effective diffusion coefficient, γ is the sticking probability [16, 25], $\Lambda^{-2} = (2.405/r)^2 + (\pi/l)^2$ is the diffusion length, and $\upsilon_T = (8\ k_B T/\pi m)^{1/2}$. All reaction pathways between the adsorbed (marked by the "s" index) and gaseous species inside R61–R66 were

assumed to be of equal probabilities. The rate coefficients for heterogeneous loss of ions R68–R70 were calculated as $k_S = \upsilon/d_c$, where $d_c = 0.5rl/(rh_l + lh_r)\,\mathrm{d_c} = 0.5\mathrm{rl}/(\mathrm{rh_l} + \mathrm{lh_r})\,\mathrm{d_c} = 0.5\mathrm{rl}/(\mathrm{rh_l} + \mathrm{lh_r})$. The correction factors for axial and radial sheath sizes are given by the low pressure diffusion theory [30].

For the effects of both gas mixing ratio and gas pressure, the calculations were performed by 10 model runs: 5 or 4 base points of T_e, n_+, J_+ and U_{dc} were directly taken from the experiment, and 5 or 6 additional intermediate points were obtained by the interpolation of the measured ones using a cubic spline procedure. Accordingly, all the model-predicted curves shown in "Results and discussion" Section result from the smooth fitting of these 10 points. Taking into account the results of previously published works [16–20], the possibility of the local non-monotonic effects between the experimental points was ignored.

For model validation, we took the experimental data on F atom density, T_e and n_e obtained by Kimura et al. [16] using optical emission actinometry and Langmuir probe measurements in the ICP reactor of similar geometry under the close range of experimental conditions. Figure 1 shows the good agreement between measured and model-predicted n_F values. Moreover, it can be seen that our model somewhat better fits their experimental data than their own model. In our opinion, such situation is provided by several reasons, and namely: (1) we used the extended reaction set for the bulk chemistry; (2) we involved the newest data set on the reaction rate coefficients from the NIST Chemical Kinetics Database [29], and (3) we accounted, though in a simplest form, for the wall chemistry of atoms and radicals. The last issue is especially important in the low-oxygenated plasmas where the heterogeneous decay of these species dominates over atom-molecular processes. At the same time, the model of Ref. [16] assumed only the loss of atoms and radicals on the reactor walls except the O → 1/2 O_2 reaction.

Modeling of Etching Kinetics

In order to analyze the relationships between plasma parameters and etching kinetics, we used the simplified phenomenological model [9, 31–33]. The assumptions were formulated as followed [20]:

1. The F atoms are the main chemically active species for SiO_2 etching process. The chemical effect from CF_x radicals was not taken into account because of much lower fluxes of these species.
2. The SiO_2 etching mechanism was assumed to be the ion-assisted chemical reaction where the role of ions includes the destruction of oxide bonds and the sputtering of the low-volatile fluorinated layer. The spontaneous chemical reaction in the F/SiO_2 system at near-to-room temperatures can be ignored because the Si–O bond (799.6 kJ/mol [34]) is much stronger than the Si–F one (552.7 kJ/mol [34]).
3. The sputtering of native (non-fluorinated) surface does not contribute the overall etching rate. The reason is that, for the given ion bombardment energies $\varepsilon_i \approx |eU_{dc}| < 160$ eV, the SiO_2 sputtering yield Y_s does not exceed 0.1 atom/ion (since $Y_s = A\left(\sqrt{\varepsilon_i} - \sqrt{\varepsilon_0}\right)$ with $A = 0.014$ eV$^{-1/2}$, and $\varepsilon_0 = 18$–20 eV [7, 9]).
4. The SiO_2 etching mechanism is not seriously affected by the fluorocarbon polymerization on the surface. First, for the given set of experimental conditions, the much higher flux of F atoms compared with ones for $CF_{x=1,\,2}$ radical provides the favorable conditions for etching, but not for polymerization. Secondly, the XPS analysis [20] indicated no sufficient increase in carbon content between the as-received

Table 1 Reaction set for the modeling of neutral species chemistry in $CF_4/Ar/O_2$ plasma

Process		Rate coefficient [cm^3/s]			
		ε_{th} [eV]	A	B	C
R1	$C_2F_4 + e = 2CF_2 + e$	3.06	1.32×10^{-8}	0.412	6.329
R2	$C_2F_4 + e = C_2F_3^+ + F + 2e$	15.57	3.03×10^{-9}	0.874	16.41
R3	$C_2F_3 + e = CF_2 + CF + e$	3.06	3.30×10^{-8}	0.412	6.329
R4	$CF_4 + e = CF_3 + F + e$	5.60	1.38×10^{-8}	0	16
R5	$CF_4 + e = CF_2 + 2F + e$	9.50	2.22×10^{-10}	0.99	14.77
R6	$CF_4 + e = CF_3^+ + F + 2e$	15.9	9.36×10^{-8}	0	20.4
R7	$CF_4 + e = CF_3 + F^+ + 2e$	23.10	9.79×10^{-10}	0.94	34.67
R8	$CF_3 + e = CF_2 + F + e$	3.80	6.48×10^{-8}	−0.959	11.25
R9	$CF_2 + e = CF + F + e$	5.40	8.11×10^{-9}	0.386	8.739
R10	$CF_2 + e = C + 2F + e$	11.00	1.39×10^{-8}	−1.164	49.87
R11	$CF + e = C + F + e$	5.60	1.63×10^{-8}	−0.002	13.05
R12	$F_2 + e = 2F + e$	4.34	1.08×10^{-8}	−0.296	4.464
R13	$O_2 + e = 2O + e$	6.40	1.52×10^{-9}	0	4.15
R14	$O_2 + e = O + O(1d) + e$	8.57	2.04×10^{-8}	0	8.18
R15	$CO_2 + e = CO + O + e$	13.50	1.87×10^{-8}	0	13.89
R16	$CO + e = C + O + e$	13.50	1.87×10^{-8}	0	13.89
R17	$O + e = O(1d) + e$	1.97	4.47×10^{-9}	0	2.29
R18	$FO + e = F + O + e$	4.30	6.16×10^{-9}	0	4.30
R19	$CFO + e = CO + F + e$	5.40	8.11×10^{-9}	0.386	8.739
R20	$CF_2O + e = CFO + F + e$	3.80	6.48×10^{-8}	−0.959	11.25
R21	$C_2F_3 + F = C_2F_4$	1.00×10^{-12}			
R22	$C_2F_4 + O = CF_2O + CF_2$	2.51×10^{-12}			
R23	$C_2F_4 + O(1d) = CF_2O + CF_2$	2.51×10^{-11}			
R24	$C_2F_4 + F = CF_2 + CF_3$	3.98×10^{-11}			
R25	$C_2F_4 + C = C_2F_3 + CF$	1.00×10^{-10}			
R26	$F_2 + CF_3 = CF_4 + F$	6.31×10^{-14}			
R27	$F_2 + CF_2 = CF_3 + F$	7.94×10^{-14}			
R28	$F_2 + CF = CF_2 + F$	3.98×10^{-12}			
R29	$F_2 + O = FO + F$	1.00×10^{-16}			
R30	$F_2 + O(1d) = FO + F$	7.94×10^{-12}			
R31	$F_2 + CFO = CF_2O + F$	5.01×10^{-14}			
R32	$CF_3 + F = CF_4$	1.00×10^{-12}			
R33	$CF_3 + O = CF_2O + F$	3.16×10^{-11}			
R34	$CF_3 + O(1d) = CF_2O + F$	3.16×10^{-11}			
R35	$CF_2 + F = CF_3$	4.17×10^{-13}			
R36	$2CF_2 = C_2F_4$	5.01×10^{-14}			
R37	$CF_2 + CF = C_2F_3$	1.00×10^{-12}			
R38	$CF_2 + O = CFO + F$	3.16×10^{-11}			
R39	$CF_2 + O(1d) = CFO + F$	3.16×10^{-11}			
R40	$CF_2 + O = CO + 2F$	3.98×10^{-12}			
R41	$CF_2 + O(1d) = CO + 2F$	3.98×10^{-12}			
R42	$CF + F = CF_2$	5.01×10^{-15}			

Table 1 continued

Process		Rate coefficient [cm^3/s]			
		ε_{th} [eV]	A	B	C
R43	$CF + O = CO + F$		6.31×10^{-11}		
R44	$CF + O(1d) = CO + F$		2.00×10^{-11}		
R45	$CF + O_2 = CFO + O$		3.16×10^{-11}		
R46	$FO + O = F + O_2$		2.51×10^{-11}		
R47	$FO + O(1d) = F + O_2$		5.01×10^{-11}		
R48	$FO + FO = 2F + O_2$		2.51×10^{-12}		
R49	$2FO = F_2 + O_2$		2.51×10^{-16}		
R50	$CFO + CF_3 = CF_4 + CO$		1.00×10^{-11}		
R51	$CFO + CF_3 = CF_2O + CF_2$		1.00×10^{-11}		
R52	$CFO + CF_2 = CF_3 + CO$		3.16×10^{-13}		
R53	$CFO + CF_2 = CF_2O + CF$		3.16×10^{-13}		
R54	$CFO + O = CO_2 + F$		1.00×10^{-10}		
R55	$CFO + O(1d) = CO_2 + F$		1.00×10^{-10}		
R56	$2CFO = CF_2O + CO$		1.00×10^{-11}		
R57	$CFO + F = CF_2O$		7.94×10^{-11}		
R58	$CF_2O + O(1d) = F_2 + CO_2$		2.00×10^{-11}		
R59	$C + O_2 = CO + O$		1.58×10^{-11}		
R60	$CO + F = CFO$		1.29×10^{-11}		
R61	$F = F(s) + CF_3 = CF_4$ $+ CF_2 = CF_3$ $+ CF = CF_2$ $+ F = F_2$ $+ C = CF$ $+ C_2F_3 = C_2F_4$ $+ O = FO$		$f(\gamma)$, $\gamma = 0.05$		
R62	$CF_3 = CF_3(s) + F = CF_4$ $+ CF = C2F_4$ $+ C = C_2F_3$		$f(\gamma)$, $\gamma = 0.05$		
R63	$CF_2 = CF_2(s) + F = CF_3$ $+ CF_2 = C_2F_4$ $+ CF = C_2F_3$ $+ O = CF_2O$		$f(\gamma)$, $\gamma = 0.1$		
R64	$CF = CF(s) + F = CF_2$ $+ CF_2 = C_2F_3$ $+ CF_3 = C_2F_4$ $+ O = CFO$		$f(\gamma)$, $\gamma = 0.1$		
R65	$C = C(s) + F = CF$ $+ CF_3 = C_2F_3$ $+ O = CO$		$f(\gamma)$, $\gamma = 1$		
R66	$O = O(s) + O = O_2$ $+ F = FO$ $+ C = CO$ $+ CF = CFO$ $+ CF_2 = CF_2O$		$f(\gamma)$, $\gamma = 0.1$		
R67	$O(1d) = O$		$f(\gamma)$, $\gamma = 1$		

Table 1 continued

Process		Rate coefficient [cm^3/s]			
		ε_{th} [eV]	A	B	C
R68	$CF_3^+ = CF_3$	υ/d_c, where			
R69	$F^+ = F$	$\upsilon \approx \sqrt{eT_e/m_i}$			
R70	$C_2F_3^+ = C_2F_3$	$d_c = 0.5rl/(rh_l + lh_r)$			

The rate coefficient for R1–R20 and R67 are from Refs. [16, 27, 28], for R21–R60 are from Ref. [29], and for R61–66 are from Refs. [16, 25]

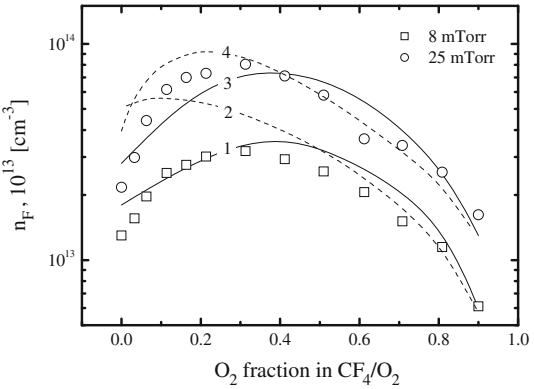

Fig. 1 Comparison of measured (*dots*) and model-predicted (*lines*) fluorine atom densities in CF_4/O_2 inductively coupled plasma: 1, 2—$p = 8$ mTorr, 3, 4—$p = 25$ mTorr. *Solid lines* represent our model while the *dashed lines* correspond to the model of Ref. [16]. The data on T_e and n_e needed for our calculations are also taken from Ref. [16]

and etched samples. Therefore, in fact, we assumed a thin steady-state (non-reactive) [35, 36] fluorocarbon layer that does not limit the transport of chemically active species to the etched surface as well as does not result in the sufficient energy loss for ions. The reasonability of these assumptions was confirmed in our earlier work [20].

According to Refs. [31, 32], the rate of ion-assisted chemical reaction can be expressed as $R = \delta s_0(1-\theta)\Gamma_F$, where δ is the stoichiometric coefficient for reaction products (for example, $\delta = 1$ for SiF, $\delta = 0.5$ for SiF_2, etc.), s_0 is the sticking coefficient for F atoms on the clean surface ($s_0 = 0.3$–0.5 for F/SiO_2 [9, 37]), θ is the fraction of fluorinated surface, $\Gamma_F \approx 0.25 n_F \upsilon_T$ is the F atom flux. The combination $\delta s_0(1-\theta)$ is known as the reaction probability. Assuming the ion-stimulated desorption (the sputtering of the fluorinated layer) to be the main pathway for cleaning the etched surface form the reaction products, the balance between free and fluorinated surface is determined by the equation of $\delta s_0(1-\theta)\Gamma_F = \theta Y_{ds}\Gamma_+$, where $\Gamma_+ \approx J_+/e$ is the total flux of positive ions, and Y_{ds} is the ion-type-averaged desorption yield. Finally, one can obtain

$$R = \delta s_0 \Gamma_F \left[1 - \frac{\delta s_0 \Gamma_F}{\delta s_0 \Gamma_F + Y_{ds}\Gamma_+}\right] \quad (2)$$

Since the parameter Y_{ds} is not known, it was used as a free variable in order to obtain the agreement between relative behaviors of experimental and model-predicted etching rates. Similarly to Y_s, the Y_{ds} was assumed to be proportional to the momentum transferred from the incident ion to the surface in a single collision [9, 31]. In order to take into account the dependence of Y_{ds} on process conditions, only the value of Y_{ds}^0 corresponding to

$p = 6$ mTorr and 50 % CF_4 + 50 % Ar gas mixture was set independently. The remaining values were calculated as $Y_{ds} = Y_{ds}^0\left(\sqrt{\varepsilon_i}/\sqrt{\varepsilon_i^0}\right)\left(m_i/m_i^0\right)$, where $\varepsilon_i \approx e|-U_f-U_{dc}|$ is the incident ion energy, and m_i is the effective ion mass. The last was simply evaluated through the mole fractions of corresponding neutral species.

Results and Discussion

From Fig. 2, it can be seen that, as the O_2 content in the $CF_4/Ar/O_2$ gas mixture increases from 0 to 50 % (i.e. as the Ar is substituted for O_2 and the transition from CF_4/Ar to CF_4/O_2 system takes place), the SiO_2 etching rate shows the non-monotonic behavior with a maximum of about 200 nm/min at 25 % Ar + 25 % O_2. The maximum etching rate is about two times higher than one obtained in CF_4/Ar plasma ($\sim$104 nm/min) and by 1.5 times exceeds the value for CF_4/O_2 plasma ($\sim$130 nm/min). An increase in gas pressure for both Ar-rich (50 % CF_4 + 38 % Ar + 12 % O_2) and O_2-rich (50 % CF_4 + 12 % Ar + 38 % O_2) gas mixtures from 4 mTorr up to 6–7 mTorr causes an increase in the SiO_2 etching rate by about 1.4 times. However, the furthermore rise of pressure turns the etching rate down, so that at $p = 10$ mTorr the etching rates appear to be close to the starting points. Therefore, similarly to the effect of Ar/O_2 mixing ratio, the change of gas pressure also causes the non-monotonic change of the SiO_2 etching rate.

Assuming the SiO_2 etching mechanism in $CF_4/Ar/O_2$ to be ion-assisted chemical reaction, one can propose two principal reasons for the non-monotonic etching rate as a function of Ar/O_2 mixing ratio and gas pressure. The first is the so-called "bulk chemistry" effect connected with the non-monotonic flux of chemically active neutrals (in our case-F atoms). Note that this reason serves as the main explanation for the non-monotonic SiO_2 etching rate in the binary CF_4/O_2 gas system in both RIE and ICP systems. The second is the so-called "surface chemistry" effect caused by the changes in reaction probability. For the ion-assisted chemical reaction with a formation of low or moderately volatile reaction products, the last parameter may be sensitive to the ion flux through the fraction of the surface acceptable for chemical reaction $(1-\theta)$. All these pathways will be analyzed below.

In order to obtain the data on plasma parameters, densities, and fluxes of active species, we used a combination of plasma diagnostics and modeling. Figure 3 represents the results of plasma diagnostics by Langmuir probes. From Fig. 3a, it can be seen that the transition from Ar-rich to O_2-rich plasma results in decreasing T_e in the range of 3.6–3.4 eV. This effect can be attributed to the increase in electron energy loss for the low-threshold electronic excitation of O_2 and other molecular species which appear in a gas phase as products of plasma chemical reactions. The same behavior of T_e with increasing gas pressure (3.6–3.45 eV for Ar-rich plasma and 3.4–3.3 eV for O_2-rich plasma at $p = 4$–10 mTorr) is also connected with increasing electron energy loss due to increasing total density of neutral species and electron-neutral collision frequency. Figures 3b, c show that an increase in O_2 content in the $CF_4/Ar/O_2$ gas mixture as well as in gas pressure reduces the values of n_+ and J_+. Particularly, as the composition of the feed gas changes from CF_4/Ar to CF_4/O_2 at constant p, the total density of positive ions (and thus, the electron density assuming $n_+ \approx n_e$) deceases from 4.2×10^{10} cm^{-3} to 3.2×10^{10} cm^{-3} that corresponds to $J_+ = 1.10$–0.95 mA/cm^2. This effect is probably caused by a combination of two phenomena. First, since an increase in O_2 content in a feed gas results in decreasing T_e, it suppresses the total ionization rate through the decreasing ionization rate coefficients for

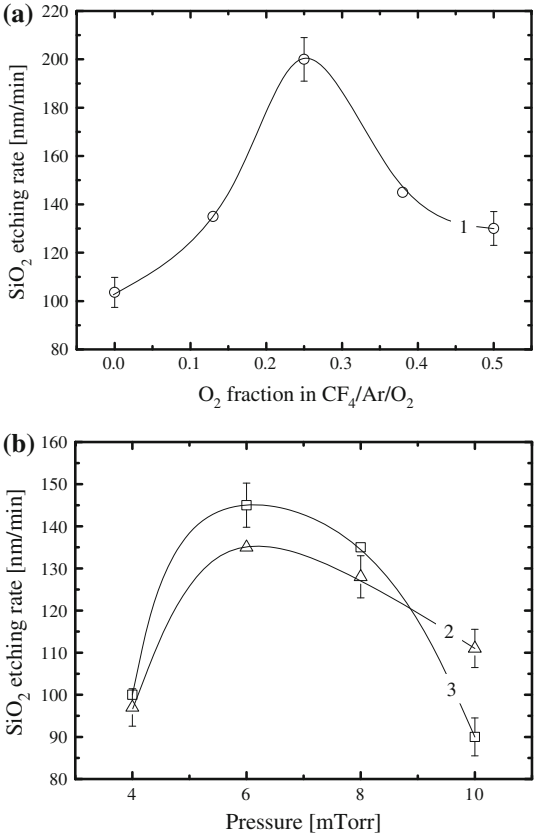

Fig. 2 Measured low-temperature SiO_2 etching rates as functions of O_2 mixing ratio (**a**) and gas pressure (**b**) at $W_{inp} = 900$ W and $W_{dc} = 200$ W: 1–$p = 6$ mTorr; 2–50 % CF_4 + 38 % Ar + 12 % O_2 gas mixture; 3–50 % CF_4 + 12 % Ar + 38 % O_2 gas mixture. The *solid lines* given by the cubic spline fitting of the experimental points are to guide the eye only

all types of neutral species. The quite high sensitivity of ionization rate coefficients to T_e is determined by the condition of $\varepsilon_{iz} \approx 12-15\,\text{eV} > (3/2)\,T_e$, where ε_{iz} is the threshold energy for ionization, and $(3/2)T_e$ is the mean electron energy [16, 28]. And secondly, an increase in O_2 content and the formation of other electronegative reaction products result in the increasing decay rates for both positive ions and electrons through ion–ion recombination and dissociative attachment, respectively. It is obviously that the effect of gas pressure works through the same pathways. Really, since an increase in gas pressure also results in decreasing T_e, the efficiency of ionization falls down. Also, as was repeatedly mentioned in published works (for example, in Refs. [24, 30, 31]), an increase in gas pressure in electronegative plasmas accelerates the decay of electrons in the dissociative attachment processes. The last is accompanied by increasing both negative ion densities and ion–ion recombination rates.

Figure 4 illustrates the influence of O_2 content in a feed gas on kinetics and densities of neutral species. In the non-oxygenated plasmas (i.e. in the 50 % CF_4 + 50 % Ar gas system), the main sources of F atoms are R4, R6, and R8 that compose about 85 % of total formation rate for this species. Among other processes resulting in formation of F atoms, the noticeable contribution comes from R12 which is supported by the high $F \rightarrow F_2$ recombination rate in R61. The remaining pathways of R61 are much less effective due to lower densities of corresponding gaseous species.

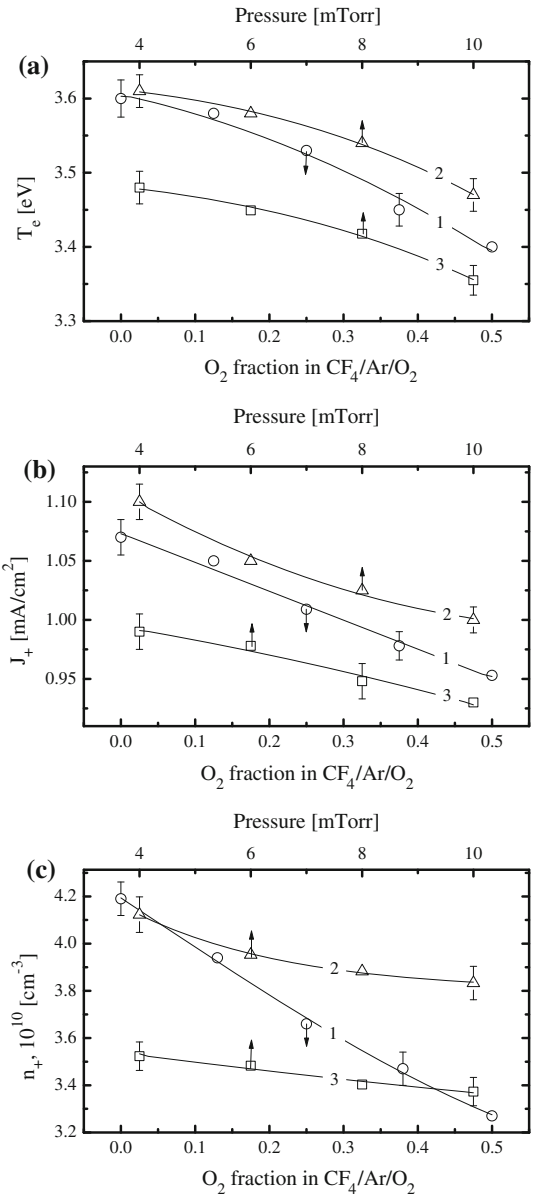

Fig. 3 Measured electron temperature **a**, ion current density **b** and total positive ion density **c** as functions of O_2 mixing ratio (1) and gas pressure (2, 3) at $W_{inp} = 900$ W and $W_{dc} = 200$ W: 1–$p = 6$ mTorr; 2–50 % CF_4 + 38 % Ar + 12 % O_2 gas mixture; 3–50 % CF_4 + 12 % Ar + 38 % O_2 gas mixture. The *solid lines* given by the cubic spline fitting of the experimental points are to guide the eye only

An increase in O_2 content in the $CF_4/Ar/O_2$ gas mixture at constant y_{CF_4} noticeably reduces the rates of R4, R6, and R8 even under the conditions of low-oxygenated ($y_{O_2} < y_{Ar}$) plasmas (for example, by 2 times at 12 % O_2). The reason is simultaneous decrease in n_e, n_{CF_4} (3.5×10^{13}–1.9×10^{13} cm^{-3} for 0–12 % O_2), and n_{CF_3} (4.9×10^{12}–1.9×10^{12} cm^{-3} for 0–12 % O_2). The density of CF_3 radicals decreases because of their decomposition in R33, R34, R50, and R51 with the participation of O, O(^{1}D) and CFO. The behavior of n_{CF_4} follows one for n_{CF_3} because the main sources of CF_4 molecules in plasma chemical reaction are the $CF_3 \rightarrow CF_4$ transformations in R61 and R62. At the same

time, the addition of O_2 introduces new channels for the formation of F atoms involving CFO (R19) and CF_2O (R20) as well as accelerates R12. The high generation rate (and thus, the density) of CFO species is provided by R20 and R60 while the CF_2O is effectively formed in R51, R56 and R57. The acceleration of R12 is due to rapidly increasing F_2 density ($n_{F_2} = 1.0 \times 10^{12}$–$9.1 \times 10^{12}$ cm^{-3} for 0–12 % O_2) because of formation of these species in R58 and R61. As a result, the total F atom formation rate increases compared with the CF_4/Ar plasma that causes an increase in F atom density ($n_F = 5.8 \times 10^{12}$–2.6×10^{13} cm^{-3} for 0–12 % O_2).

The furthermore addition of O_2 in a feed gas and the transition to the high-oxygenated ($y_{O_2} > y_{Ar}$) plasmas keep all mentioned tendencies for reaction rates as well as introduce more mechanisms for the formation of F atoms. Particularly, in the 50 % CF_4 + 50 % O_2 gas mixture ($y_{O_2} = 0.5$ and $y_{Ar} = 0$) the rate of electron impact dissociation of FO species (R18) stands together with R19 and R20 and exceeds the total effect of R4, R6, and R8. The high formation rate and density of FO (8.1×10^{10}–6.4×10^{12} cm^{-3} for 12–50 % O_2) are mainly provided by R30, R61 and R66. Also, the rates of atom-molecular processes R30, R46–R48, and R54 increase together with increasing O_2 content in a feed gas and, finally, appear to be comparable with R18–R20. As can be seen from Fig. 4a, such situation leads to the monotonic increase (thought with some saturation effect) in F density because of the same behavior of total F atom formation rate. Therefore, the substitution of Ar by O_2 at constant CF_4 fraction in CF_4/Ar/O_2 gas mixture does not result in non-monotonic behavior of F atom density. Note that the opposite tendencies of F and CF_x densities with increasing O_2 content in a feed gas create a favorable condition for etching, not for polymerization.

The data discussed above allow one to define clearly the differences between the three-component CF_4/Ar/O_2 (with constant y_{CF_4}) and "classical" two-component CF_4/O_2 gas systems. In the CF_4/O_2 gas mixture, the addition of O_2 at constant p results in a proportional decrease of CF_4 fraction in a feed gas. This fact results in a faster decrease in the densities of both CF_4 and CF_3 (compared with those mentioned by Fig. 4a) as well as in slower increase in F_2, CFO, CF_2O, and FO densities. In fact, the formation rates for these species appear to be strongly limited by the lack of fluorine coming with the feed gas. As a result, the densities of F_2, CFO, CF_2O, and FO exhibit maximums in the range of 30–50 % O_2 that is directly reflected on the behavior of the F atom density through the non-monotonic rates of R12, R18–R20 and R46–R48.

The behaviors of species densities versus gas pressure were found to be similar for any fixed feed gas composition. In order to avoid repetitions, the modeling data in Fig. 5 and the subsequent discussion are related to the highly-oxygenated plasma (50 % CF_4 + 12 % Ar + 38 % O_2) only. In spite of increasing amount of CF_4 molecules in a feed gas, the densities of all CF_x species, including the CF_4 itself, demonstrate a decrease with increasing gas pressure (for example, $n_{CF_4} = 8.1 \times 10^{10}$–$6.4 \times 10^{12}$ cm^{-3} and $n_{CF_3} = 8.1 \times 10^{10}$–$6.4 \times 10^{12}$ cm^{-3} for 4–10 mTorr). Since the recombination of fluorocarbon radicals in both bulk and surface reactions follow the general pathway $CF_{x-1} \rightarrow CF_x$, the density of higher-saturated species is closely connected with the density of lower-saturated ones. An increase in gas pressure directly reduces the density of CF through their interaction with O_2 molecules in R45, and the decrease in n_{CF} pre-determines the similar tendencies for other CF_x species. The processes with the participation of O and O(^{1}D) do not work by the same way because of decreasing O_2 dissociation degree toward higher pressures. As a result, a growth of n_O appears to be much slower than that for n_{O_2}. It was found also that an increase in gas pressure does not influence principally the F atom

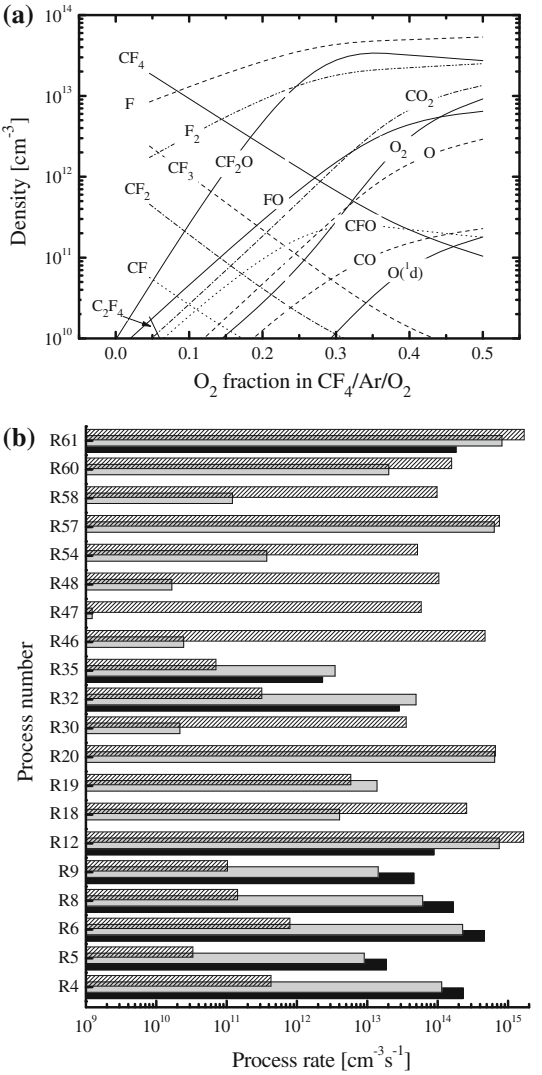

Fig. 4 Model-predicted densities of neutral species **a** and the main formation-decay processes for F atoms **b** as functions of O_2 mixing ratio. In **a** and **b** $p = 6$ mTorr, $W_{inp} = 900$ W and $W_{dc} = 200$ W. In **b** *black bars* are for 0 % O_2, gray bars correspond to 12 % O_2, and the *patterned bars* correspond to 50 % O_2

formation kinetics. Similarly to the previous case, in both low and high pressure ends the main sources of F atoms are R12, R18–R20 and R46–R48. The monotonic increase in their rates provides the monotonic change in F atom density in both Ar-rich ($n_F = 1.8 \times 10^{13}$–4.2×10^{13} cm^{-3} for 4–10 mTorr) and O_2-rich ($n_F = 3.3 \times 10^{13}$–8.2×10^{13} cm^{-3} for 4–10 mTorr) plasmas. Again, since the densities of F and CF_x change by the opposite ways as shown in Fig. 5a, an increase in gas pressure assists in the suppression of the polymerization.

When analyzing the plasma chemistry in the Ar-containing plasmas, one must remember about the possibility of stepwise bulk processes involving metastable atoms Ar ($^3P_{0\text{-}2}$), further denoted as Ar^m. Since the free energy of these species ε_m is about 11.6–11.8 eV [38, 39], generally we can expect the contribution of stepwise dissociation for all

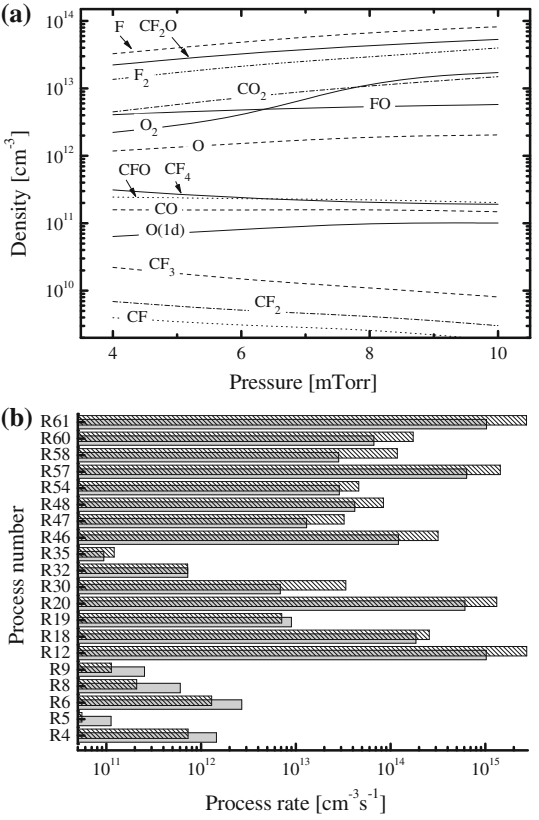

Fig. 5 Model-predicted densities of neutral species **a** and the main formation-decay processes for F atoms **b** as functions gas pressure for 50 % CF_4 + 12 % Ar + 38 % O_2 gas mixture. In **a** and **b** at $p = 6$ mTorr, $W_{inp} = 900$ W and $W_{dc} = 200$ W. In **b** the gray bars correspond to 4 mTorr, and the patterned bars correspond to 10 mTorr

molecular species which satisfy the condition $\varepsilon_{th} < \varepsilon_m$, where ε_{th} is the threshold energy for dissociation shown in Table 1. Here, the species of primary interest are the CF_4 and CF_3 (as the main primary sources of F atoms) as well as the O_2 molecules providing the formation of FO, CFO and CF_2O. According to Ref. [39], the rate coefficient for the electron impact excitation of Ar^m can be expressed as $5.0 \times 10^{-9} T_e^{0.74} exp\,(-11.56/T_e)$ that gives $k_m = 5.2 \times 10^{-10}$–$4.1 \times 10^{-10}$ cm^3/s for 0–50 % O_2 at $p = 6$ mTorr. The maximum rate of this process of about 8.5×10^{14} cm^{-3} s^{-1} corresponds to the non-oxygenated ($y_{Ar} = 0.5$ and $y_{O_2} = 0$) CF_4/Ar plasma and appears to be comparable with the total effect of R4, R6 and R8 ($\sim 8.8 \times 10^{14}$ cm^{-3} s^{-1}). Therefore, assuming that all Ar^m species are deactivated in the dissociative interactions with CF_4 and CF_3, the about 50 % contribution of the stepwise dissociation to the total F atom formation rate seems to be possible. However, in practice, we expect such contribution to be much lower, even negligible. The reason is the fast heterogeneous loss of Ar^m which, at low pressures, dominates over other decay channels. Really, when taking the rate coefficients for $CF_4 + Ar^m = CF_3 + F + Ar$ and $CF_3 + Ar^m = CF_2 + F + Ar$ from Ref. [18] as $k_q = 6.0 \times 10^{-11}$ cm^3/s, one can easily obtain that $k_q(n_{CF_4} + n_{CF_3}) \ll k_{s,Ar^m} 5 \times 10^3$ s^{-1}, where k_{s,Ar^m} is the rate coefficient for the heterogeneous loss of Ar^m given by Eq. (1) with $\gamma = 1$ [21, 39]. The last conclusion is directly confirmed by the experimental data of Hioki et al. [40]. Particularly, they have found that there are no changes in both density and spatial profiles of Ar^m with the additions of CF_4 to Ar plasma at $p = 5$–15 mTorr while such changes take place at

$p > 50$ mTorr. The negligible role of Ar^m in the CF_x dissociation kinetics was also mentioned in Ref. [25] for the CF_4/Ar ICP under the close range of experimental conditions and reactor geometry. It is evidently clear that the substitution of Ar by O_2 in the CF_4/Ar/O_2 gas mixture lowers the Ar^m excitation rate, so that at 10–12 % O_2 the gap between R_m and the sum of R_4, R_6, R_8, R_{12}, R_{19} and R_{20} reaches an order of magnitude. The noticeable stepwise dissociation of O_2 molecules can principally be possible at low O_2 contents, when $k_m n_{Ar} \gg (k_{13} + k_{14}) n_{O_2}$. The simple evaluations show that, since the condition $k_m n_{Ar} = (k_{13} + k_{14}) n_{O_2}$ takes place at $y_{O_2} = 0.08$, the stepwise dissociation of O_2 can contribute the total formation rate for oxygen atoms only when the O_2 content in the gas mixture is less than 1 %. For such mixtures, even the complete dissociation of O_2 does not influence the kinetic and density of F atoms. All these allow one to conclude that, for the given set of experimental conditions, the stepwise processes involving Ar metastable atoms are not effective.

The data on plasma composition reported above allows one to analyze the SiO_2 etching mechanism using the relationships and assumptions discussed in "Modeling of etching kinetics" section. From Eq. (2), it can be seen that the condition $\delta s_0 \Gamma_F \ll Y_{ds} \Gamma_+$ gives $\theta \to 0$ (clean surface) and $R \approx \delta s_0 \Gamma_F$ that corresponds to the neutral-flux-limited etching regime. In this regime, assuming constant δs_0 at constant surface temperature, one can expect a monotonic increase in the SiO_2 etching rate with both O_2 fraction and gas pressure following the behavior of F atom flux (Fig. 6a). Oppositely, the condition $\delta s_0 \Gamma_F \gg Y_{ds} \Gamma_+$ provides $\theta \to 1$ (fluorinated surface) and $R \approx Y_{ds} \Gamma_+$. A small increase in $\sqrt{\varepsilon_i}$ (which is mainly determined by the behavior of U_{dc} (Fig. 6c), since $U_{dc} \gg U_f$) with increasing both O_2 fraction and gas pressure is almost completely compensated by the decreasing effective ion mass. As a result, the Y_{ds} appears to be a very weak function of mentioned operating parameters (for example, $Y_{ds} = 4.2$–4.3 for Ar-rich gas mixture and 3.6–3.7 for O_2-rich gas mixture at $p = 4$–10 mTorr and $Y_{ds}^0 = 4.5$), and the SiO_2 etching rate should follow the monotonic behavior of Γ_+ (Fig. 6b). In our case, since the monotonic fluxes of both F atoms and positive ions has no direct correlation with the behavior of the SiO_2 etching rate, no one pure etching regime is realized. Therefore, for the given set of experimental conditions, we consider the transitional regime of ion-assisted chemical reaction where the etching rate is controlled by neutral and ion fluxes together and which is described by the full Eq. (2). From Fig. 7, it can be seen that, at $Y_{ds}^0 = 5$, Eq. (1) provides the reasonable agreement between model-predicted and measured relative etching rates. In our opinion, the value of $Y_{ds}^0 = 5$ look quite rational though it exceeds the Ar^+ ion induced SiO_2 sputtering yield by more than an order of magnitude. The reason is that the sputtering of the partially fluorinated layer appears to be much easier (i.e. with lower threshold energy) compared with the original SiO_2 surface. The similar results were obtained in Refs. [9, 31, 32]. The model-based analysis of etching kinetics allows one to explain the non-monotonic SiO_2 etching rates as follows. In CF_4/Ar plasma, the etching process occurs with a relatively clean surface ($\theta - 0.3$, see Fig. 7a) and thus, is closer to the neutral-flux-limited etching regime. An increase in the O_2 fraction in a feed gas causes increasing fluorination rate (through increasing Γ_F) and simultaneously retards the ion-stimulated desorption of reaction products (through decreasing Γ_+). All these result in increasing fraction of fluorinated surface ($\theta = 0.3$–0.9 for 0–50 % O_2 at $p = 6$ mTorr) and thus, in decreasing reaction probability $\delta s_0 (1 - \theta)$. And namely the combination of increasing Γ_F and decreasing reaction probability creates the non-monotonic behavior of the SiO_2 etching rate. It should be noted also that, for the given Γ_F and Γ_+, the value $\theta = 0.5$–0.6 serves as a border between the neutral-flux and ion-flux-limited etching regimes. Therefore, one can

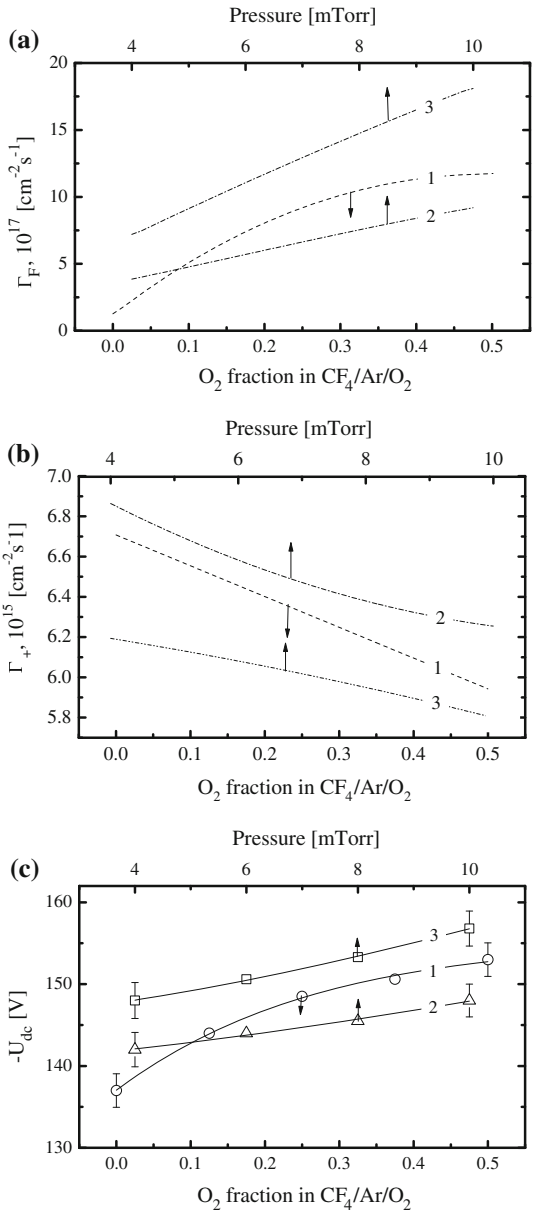

Fig. 6 Model-predicted fluxes of fluorine atoms **a**, positive ions **b** and measured negative dc bias voltage **c** as functions of O_2 mixing ratio (1) and gas pressure (2, 3) at $W_{inp} = 900$ W and $W_{dc} = 200$ W: 1–$p = 6$ mTorr; 2–50 % CF_4 + 38 % Ar + 12 % O_2 gas mixture; 3–50 % CF_4 + 12 % Ar + 38 % O_2 gas mixture

say also that an increase in the O_2 fraction in a feed gas results in the transition between neutral-flux and ion-flux-limited etching regimes while the non-monotonic etching rate is because of the opposite changes of Γ_F and Γ_+.

Since the variation of gas pressure for both Ar-rich and O_2-rich gas mixtures also results in the opposite behaviors of Γ_F and Γ_+, the changes in the etching mechanism have no principal differences with the effect of gas mixing ratio discussed above. We would like to note only that, though the model demonstrates principally the non-monotonic effect of gas

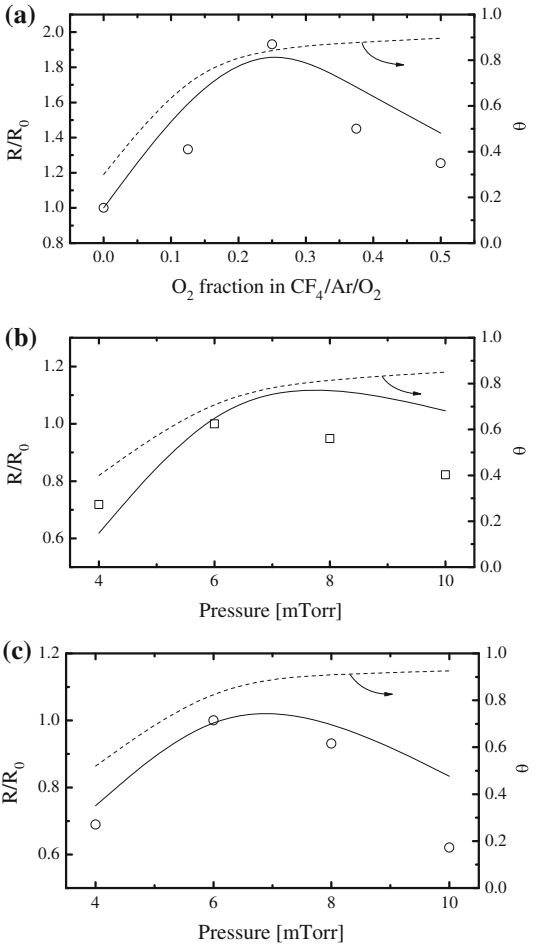

Fig. 7 Comparison of measured (*dots*) and model-predicted (*lines*) relative SiO_2 etching rates as functions of O_2 mixing ratio **a** and gas pressure **b**, **c** at $W_{inp} = 900$ W and $W_{dc} = 200$ W. In (**a**) $p = 6$ mTorr, R_0 corresponds to 0 % O_2. In (**b**) 50 % $CF_4 \pm 38$ % Ar $\pm$ 12 % O_2 gas mixture, R_0. Corresponds to 6 mTorr. In **c** 50 % $CF_4 \pm 12$ % Ar $\pm$ 38 % O_2 gas mixture, R_0 corresponds to 6 mTorr. The model parameters are $\delta s_0 = 0.2$, $Y^0_{ds} = 5$. The *dashed lines* represent the fraction of fluorinated surface θ

pressure on the SiO_2 etching rate, the agreement with experiments is worse than that for the effect of gas mixing ratio. In our opinion, such situation is because of many model simplifications. Particularly, the accounting for an increasing gas temperature in the range of 600–900 K for 4–10 mTorr (parametrically, not from the experiment) makes Figs. 7b, c to be much better. The reason is that the Γ_F increases faster (3.5×10^{17}–1.1×10^{18} cm^{-2} s^{-1} for 12 % O_2 and 6.6×10^{17}–2.1×10^{18} cm^{-2} s^{-1}, i.e. by about 3.1 times) than that at constant T (by about 2.4, see Fig. 6a). As a result, the maximum on the model-predicted etching rate appears at lower pressures (due to faster saturation of the etched surface by the reaction products) while the etching rate itself falls deeper after reaching the maximum. For example, one can obtain $R/R_0 \sim 0.9$ for low-oxygenated (12 % O_2) plasma and ~ 0.7 for high-oxygenated (38 % O_2) plasma at $p = 10$ mTorr. It is clear that these model-predicted values are much closer to the experimental ones (0.82 and 0.62, respectively) than those shown by the solid lines in Fig. 6 b,c.

Finally, we would like to note that the described model provides rather qualitative than quantitative analysis of the SiO_2 etching mechanism because of many limitations in primary assumptions. At the same time, the model clearly demonstrates how the system with

opposite monotonic changes in both ion and chemically active neutral fluxes can result in the non-monotonic etching rate.

Conclusions

In this work, we investigated how the feed gas composition (Ar/O_2 mixing ratio at constant 50 % CF_4 fraction) and gas pressure influence plasma parameters, densities of active species, and the etching mechanism for low-temperature SiO_2 films in the $CF_4/Ar/O_2$ inductively coupled plasma. It was found that that an increase in O_2 content in the $CF_4/Ar/O_2$ gas mixture in the range of 0–50 % (i.e. the transition from CF_4/Ar to CF_4/O_2 system) results in the non-monotonic SiO_2 etching rate. Similar effect was also found for the change in gas pressure from 4 to10 mTorr at any fixed feed gas composition. The zero-dimensional plasma model with Langmuir probe diagnostics data showed that the densities and fluxes of F atoms and positive ions exhibit opposite monotonic behaviors versus chosen input parameters. The model-based analysis of etching kinetics demonstrated that the non-monotonic effects of the SiO_2 etching rate are connected with the decrease in the reaction probability and with the transition from neutral-flux to ion-flux-limited regimes of ion assisted chemical reaction, but do not result from with the non-monotonic change of fluorine atom density, as was found in several works for the binary CF_4/O_2 system.

Acknowledgments This work was supported by the Industrial Strategic Technology Development Program (10041681, Development of fundamental technology for 10 nm process semiconductor and 10 G size large area process with high plasma density and VHF condition) funded by the Ministry of Knowledge Economy (MKE, Korea).

References

1. Wolf S, Tauber RN (2000) Silicon Processing for the VLSI Era, vol 1. Prosess Technology, Lattice Press, New York
2. Rossnagel SM, Cuomo JJ, Westwood WD (eds) (1990) Handbook of plasma processing technology. Noyes Publications, Park Ridge, NJ
3. Lindroos V, Tilli M, Lehto A, Motooka T (2010) Handbook of silicon based MEMS materials and technologies. William Andrew Applied Science Publishers, Oxford
4. Lyshevski SE (2002) MEMS and NEMS: systems, devices, and structures. CRC Press, New York
5. Rooth JR (1995) Industrial plasma engineering. IOP Publishing LTD, Philadelphia
6. Coburn JW (1982) Plasma etching and reactive ion etching. AVS Monograph Series, New York
7. Chapman B (1980) Glow discharge processes: sputtering and plasma etching. John Wiley & Sons, New York
8. Roosmalen AJ, Baggerman JAG (1991) S. J. H. Brader Dry etching for VLSI. Plenum Press, New York
9. Gray DC, Tepermeister I, Sawin HH (1993) J Vac Sci Technol A 11:1243
10. Winters HF, Coburn JW, Chuang TJ (1983) J Vac Sci Technol B 1:469
11. Mogab CJ, Adams AC, Flamm DL (1978) J Appl Phys 49:3796
12. Butterbaugh JW, Gray DC, Sawin HH (1991) J Vac Sci Technol B 9:1461
13. Smolinsky G, Flamm DL (1979) J Appl Phys 50:4982
14. Chen M, Minkiewicz VJ, Lee K (1979) J Electrochem Soc 126:194
15. Knizikevičius R (2010) Acta Phys Pol A 117:478
16. Kimura T, Noto M (2006) J Appl Phys 100:063303
17. Plumb IC, Ryan KR (1986) Plasma Chem Plasma Proc 6:205
18. Venkatesan SP, Trachtenberg I, Edgar TF (1990) J Electrochem Soc 137:2280
19. Schoenborn Ph, Patrick R, Baltes HP (1989) J Electrochem Soc 136:199
20. Kim M, Min N-K, Efremov A, Lee HW, Park C-S, Kwon K-H (2008) J Mater Sci: Mater Electron 19:957

21. Kimura T, Hanaki K (2008) Jpn J Appl Phys 47:8546
22. Johnson EO, Malter L (1950) Phys Rev 80:58
23. Sugavara M (1998) Plasma etching: fundamentals and applications. Oxford University Press, New York
24. Efremov A, Min N-K, Choi B-G, Baek K-H, Kwon K-H (2008) J Electrochem Soc 155:D777
25. Efremov AM, Kim D-P, Kim C-I (2004) Vacuum 75:133
26. Kimura T, Ohe K (1999) Plasma Sources Sci Technol 8:553
27. Kimura T, Ohe K (2002) J Appl Phys 92:1780
28. Bose D, Rauf S, Hash DB, Govindan TR, Meyyappan M (2004) J Vac Sci Technol A 22:2290
29. NIST Chemical Kinetics Database http://kinetics.nist.gov/kinetics/index.jsp
30. Lieberman MA, Lichtenberg AJ (1994) Principles of plasma discharges and materials processing. Wiley, New York
31. Lee C, Graves DB, Lieberman MA (1996) Plasma Chem Plasma Proc 16:99
32. Efremov AM, Kim DP, Kim CI (2004) IEEE Trans Plasma Sci 32:1344
33. Efremov AM, Kim DP, Kim CI (2005) Thin Solid Films 474:267
34. Lide DR (1998–1999) Handbook of chemistry and physics. CRC Press, New York
35. Schaepkens M, Standaert TEFM, Rueger NR, Sebel PGM, Oehrlein GS, Cook JM (1999) J Vac Sci Technol A 17:26
36. Zhang D, Kushner MJ (2001) J Vac Sci Technol A 19:524
37. Kwon O, Bai B, Sawin HH (2006) J Vac Sci Technol A 24:1920
38. Gudmundsson JT (2001) Plasma Sources Sci Technol 10:76
39. Ashida S, Lee C, Lieberman MA (1995) J. Vac. Sci. Technol. A 13(5):2498
40. Hioki K, Hirata H, Matsumura S, Lj. Petrović Z, Makabe T (2000) J Vac Sci Technol A 8(3):864